AUTOMATIC MASK GENERATION USING INDEPENDENT COMPONENT ANALYSIS IN DYNAMIC CONTRAST ENHANCED-MRI

Hatef Mehrabian[*1], *Ian Pang*[1], *Chaitanya Chandrana*[1], *Rajiv Chopra*[1] *and Anne L. Martel*[1]

[1]Department of Medical Biophysics, University of Toronto, Toronto, ON, Canada

ABSTRACT

Studying image intensity change in each pixel in dynamic contrast enhanced (DCE)-MRI data enables differentiation of different tissue types based on their difference in contrast uptake. Pharmacokinetic modeling of tissues is commonly used to extract physiological parameters (i.e. K^{trans} and v_e) from the intensity-time curves. In a two compartmental model the intensity-time curve of the feeding blood vessels or arterial input function (AIF) as well as the signal from extravascular space (ES) is required. As direct measurement of these quantities is not possible some assumptions are made to approximate their values. Any error in measuring these quantities results in an error in the measured physiological parameters. We propose using Independent component analysis (ICA) to generate an automatic mask for separating the two spaces and extracting their intensity-time curves. An experimental phantom is constructed to mimic the behavior of real tissues and the actual intensity-time curves for the AIF and ES are measured from its DCE-MRI images. Then ICA is applied to the DCE dataset to separate these spaces. The result show high degree of agreement between the actual and ICA results.

Index Terms— Independent Component Analysis, Pharmacokinetic modeling, Dynamic Contrast Enhanced-MRI.

1. INTRODUCTION

Dynamic contrast enhanced (DCE)-MRI has become a useful tool in studying many tumors such as in evaluating head and neck cancers, differentiating tumor from non-tumor in the cervical lymph nodes or lymphoma from squamous cell carcinoma [1-3]. A conventional DCE-MRI study involves intravenous injection of a contrast agent i.e. gadolinium (Gd) immediately prior to acquiring a sequence of images. The presence of contrast agent in each voxel causes an increase in the recorded MR signal that can be observed over the time course of the experiment. The rate with which the contrast agent passes from the intravascular space into the interstitial space is a determinant of several factors such as tumor perfusion, vascular density, and vascular permeability. MRI signal changes depend on these factors and also the leakage (interstitial) space [4].

Studying such concentration-time curves enables identification of different tissue types due to their difference in contrast uptake properties [5]. Typically, cancerous tissue is expected to show a high and fast uptake due to a proliferation of leaky angiogenic microvessels, while normal tissue shows little or slow uptake. However due to heterogeneity of the tumor vasculature contrast agent might not be able to reach some areas of the tumor vasculature.

Pharmacokinetic (PK) modeling of DCE-MRI data has emerged as a standard method for understanding tissue physiology in cancer imaging, cardiac and cerebral perfusion, inflammatory disorders, etc. [6, 7]. The contrast uptake curves are often fitted using a PK model to give a physiologically relevant parameterization of the curves. Study of these curves or parameters has been used clinically to identify and characterize tumors into malignant or benign classes. A standard approach for quantitatively modeling DCE-MRI data is a two-compartment model, with separate compartments for the blood plasma and extravascular space (ES). The parameters of the model, K^{trans} and v_e, are shown to be clinically relevant and have been used in various imaging techniques for tumor detection and to evaluate response to therapy [2, 8].

One of the main difficulties in PK modeling of tissue response is the need for measurement of the arterial input function (AIF) and the contrast concentration in ES. Any error in measuring these quantities results in error in the measured PK parameters [9]. Conventionally, due to the difficulty in measuring AIF at the tissue of interest (this signal is mixed with the ES signal in tissue), the contrast concentration in a major artery close to the tissue of interest is used as an approximation of AIF. In other cases where measuring the signal from feeding artery is difficult, a population-averaged AIF is used in the model [10]. The ES signal is also approximated by subtracting this AIF signal from the average contrast agent concentration of the tissue.

In this study we have constructed an experimental phantom to model the AIF and ES compartments of real tissues. The phantom is made such that a binary mask can be generated using pre-contrast images to separate pixels that lie inside the vessels and is used to validate our approach. However in real cases, due to the partial volume effect, the inside and outside of the vessels are mixed such that neither a mask nor a region of interest can be generated. The goal of this study is to develop an independent component analysis (ICA) based technique to automatically generate a mask to

identify and separate the AIF and ES signals using the signal that is measured in the target tissue (the site that leaking is taking place). Having a linear combination of the two signals [11, 12] that are spatially independent i.e. there is no overlap between the two spaces anatomically, ICA is capable of identifying them based on the difference in their contrast uptake dynamics. This provides a more accurate model as it uses the exact values of AIF and ES signals.

2. THEORY AND METHODS

2.1. Experimental phantom

A leaky phantom for contrast imaging was constructed to mimic the behavior of contrast agent *in vivo*, i.e. the MR Gd-chelates diffuse freely between the intravascular and extravascular spaces. The phantom consists of a chamber of agar gel (tissue mimicking material), through which small porous tube that represent the microvessels, path through parallel to each other.

Dialysis tubing (Diapes PES-150, Baxter, ID = 200 μm, wall thickness = 30 μm) was used due to its permeability and size. The tubes approximate the diameter of small arteries or large arterioles, their length was about 25mm to provide large imaging region and their pore size is between 89 and 972nm enabling low-molecular weight tracers for MR to diffuse out. The tubes were arranged in a 10x10 grid with center to center spacing of 300 μm between the tubes. The inner volume of the container around the tubes was filled with agar (0.5 wt**%,** Sigma-Aldrich Canada Ltd., Canada) by slowly injecting liquid agar between 50-60°C. The phantom is shown in figure 1.

Figure 1 the phantom that is constructed to mimic the tissue with blood vessels and extravascular space

2.2 MR data acquisition

Dynamic contrast enhanced MRI (DCE-MRI) was performed on a 1.5T scanner (Signa, GE Healthcare, USA) using a custom-made single channel RF receive coil enabling high resolution imaging of the phantom. In order to segment the compartments within the phantom, i.e. inside/outside the tubes, a high SNR image (TR = 12.5 ms, TE = 2.9 ms, Flip Angle = 20, BW = 15.63 kHz, Nx/Ny/NEX = 256/256/5, FOV = 45 mm, Slice Thickness = 5 mm) was acquired transverse to the phantom which was used in subsequent analysis as a mask (shown in figure 2). These results are used as the actual values in validating the results of separation using ICA.

The contrast agent Omniscan (GE Healthcare, USA) was diluted with de-ionized water (50:50 volume ratio) and injected into the flow line within a 0.1 ml bolus at 1 ml/s using a 2ml flush and an MR compatible pump (Spectris Solaris EP, MEDRAD Inc., Warrendale, USA). Dynamic contrast-enhanced imaging was performed using a 2D fSPGR acquisition (TR = 12.5 ms, TE = 2.9 ms, Flip Angle = 20, BW = 15.63 kHz, Nx/Ny/NEX = 256/256/1, FOV = 45 mm, Slice Thickness = 5 mm) where 256 images were acquired over about 14 minutes with a temporal resolution of 3.3 s and no delay between acquisitions.

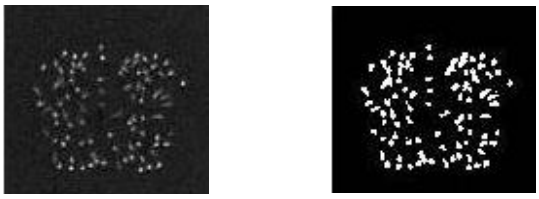

(a) (b)

Figure 2 a) the actual MR image of the mask that is acquired prior to administration of contrast agent, b) the binary mask that is generated to differentiate the tubes from the gel.

The DCE-MR image sequence was reconstructed in two different resolutions. The first dataset is reconstructed using the full k-space data (256×256), in the other dataset high frequency elements are eliminated and a low resolution dataset is reconstructed using a 64×64 matrix in k-space. A sample frame of each dataset is shown in Figure 3. These different datasets are generated to account for different resolutions that are commonly encountered in clinical trials.

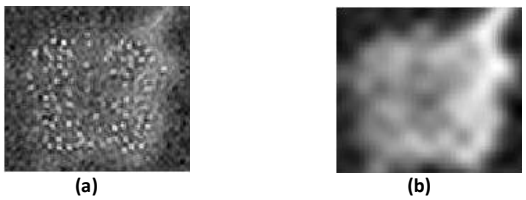

(a) (b)

Figure 3 A sample frame of the three datasets, a) high resolution (full k-space) and, b) low resolution (64 by 64 in k-space)

2.3 Independent Component analysis (ICA)

Independent component analysis (ICA) is a statistical signal processing approach that aims to extract underlying features of the dataset (unobserved components or source signals) from observed mixtures such that the extracted features are mutually independent, without assuming any knowledge of the mixing coefficients [13]. ICA is motivated from blind source separation problem for data models of the form

$$X = AS \quad (1)$$

where $X = [x_1, x_2, \dots, x_N]^T$ is a matrix of the N observed mixtures (frames or images), $S = [s_1, s_2, \dots, s_M]^T$ is a matrix containing the M source signals, independent

components or IC's (usually $M \leq N$) and $A \in \mathbb{R}^{N\times M}$ is the mixing matrix. The aim of ICA is to estimate the independent components S and the mixing matrix A having the observed mixture signals X. Classical ICA algorithms try to find an unmixing matrix $W \in \mathbb{R}^{M\times N}$ and estimate the IC matrix $Y = [y_1, y_2, \dots, y_M]^T$ such that:

$$Y = WX \quad (2)$$

where rows of Y are statistically independent. The IC's can be recovered up to scaling and permutation [14].

2.4 Separating AIF from ES

A one-unit ICA approach with negentropy as the nongaussianity measure is used to separate the AIF and ES signals [14]. The one-unit ICA approach enables extracting one IC at a time and a total of 6 IC's are estimated for each dataset. It was observed that 3 IC's appear to correspond to the AIF and ES signals and that one of these IC's appear to represent the AIF (peaks earlier and washes out faster) and the other two represent the ES signal. These 3 IC's that are selected manually from the 6 estimated ones are shown for the high resolution dataset in figure 4.

To account for the scaling ambiguity of ICA, a binary mask is generated using each estimated IC image. A threshold is selected for each IC image (50% of its highest signal intensity) and its corresponding mask is generated. Each mask is then multiplied by every frame in the original dataset to separate the signal corresponding to that component from the rest of the data. For the case of AIF (figure 4a) these segmented images are finally averaged for each frame and the intensity-time curves of each component are measured. In case of the ES (figure 4b and c), since the combination of the two components represent the ES signal, the two segments are added and the average of their sum is used as the intensity-time curve of the ES signal.

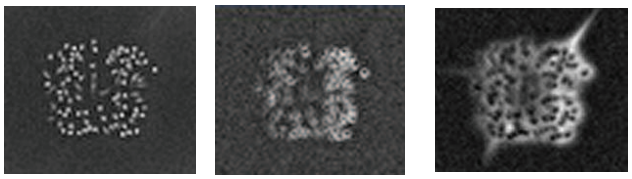

(a) (b) (c)

Figure 4 The 3 IC's that are estimated for the high resolution dataset that represent a) AIF, b) ES part 1 and, c) ES part 2

3. RESULTS

3.1 Phantom study

The AIF and ES signals are extracted from the 3 IC's using the method described in section 2.4. The two compartments as well as their corresponding intensity-time curves for the dataset that was reconstructed using the full k-space data (256×256 in k-space) are shown in Figure 5a, b and c respectively. As the actual values of the intensity-time curves are not required in the PK models and they only use their relative values, the intensity-time curves are normalized with respect to the maximum value of the AIF (tubes) curve to make it easier to compare them with the mask data. Furthermore; to make the curves of the two methods comparable the bias values are subtracted from these curves (signal intensity is considered zero before administration of contrast agent). In Figure 6 the extracted IC's and their corresponding intensity-time curves for the low resolution dataset (64×64 in k-space) are shown.

As mentioned in the experimental data acquisition section, a mask was generated to separate the tubes from their surrounding tissue. The intensity-time curves that are extracted from the images using this mask represent the actual signal intensity changes in the two regions (tubes and their surrounding tissue) of the phantom. These intensity-time curves for the high and low resolution datasets are shown in figure 7a and b respectively.

The ratio of the peak value of the AIF to ES signals is given in Table 1. Table 2 reports the full width at half maximum (FWHM), the onset time and the time to peak intervals for each intensity-time curve for both ICA and mask results.

Table 1 Ratio of the peak value of AIF to ES signal

	High Resolution	Low Resolution
ICA	2.13	2.34
Actual (mask)	2.01	2.23

Table 2 the full width at half maximum (FWHM), the onset time and the time to peak intervals for each intensity-time curve

	Tubes (Actual)	Tubes (ICA)	Leakage (Actual)	Leakage (ICA)
	Full width at half maximum of the curves [min]			
High Resolution	1.73	1.46	5.46	3.51
Low Resolution	2.6	2.22	5.35	4.86
	Time to peak of the curves [min]			
High Resolution	1.46	1.46	1.99	1.99
Low Resolution	1.62	1.62	1.95	1.99
	Onset time of the curves [min]			
High Resolution	0.76	0.76	0.86	0.86
Low Resolution	0.81	0.76	0.86	0.91

3.2 In vivo experiment

The proposed separation technique was also evaluated in vivo using rabbit as the animal model with a tumor in its thigh muscle. The DCE-MR image acquisition was performed on a 1.5T scanner (Signa, GE Healthcare, USA). The contrast agent was administered intravenously and imaging was performed immediately after injection.

A total of 200 frames (TR = 6.9 ms, TE = 2.4 ms, Flip Angle = 30, BW = 15.63 kHz, Nx/Ny/NEX = 256/256/4, FOV = 15cm, Slice Thickness = 2mm) were acquired with a temporal resolution of 2.7s per frame [15].

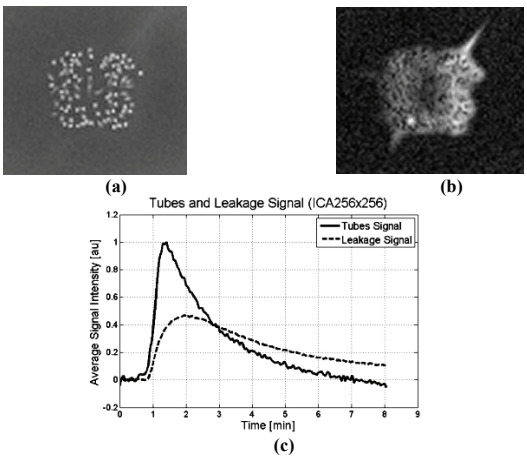

Figure 5 Results of applying ICA to the high resolution dataset, a) The tubes signal (AIF), b) the leakage signal (ES), c) the intensity-time curve corresponding to the two compartments.

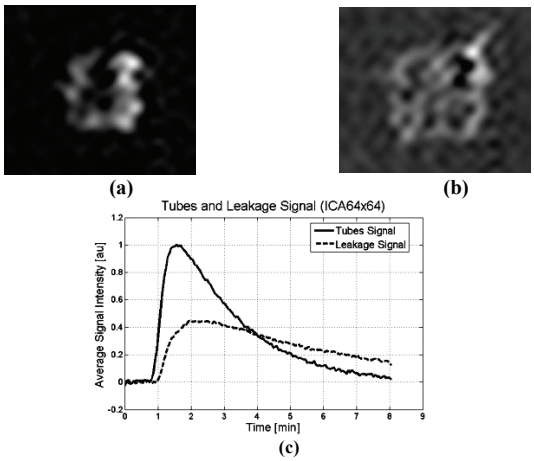

Figure 6 Results of applying ICA to the low resolution dataset, a) The tubes signal (AIF), b) the leakage signal (ES), c) the intensity-time curve corresponding to the two compartments.

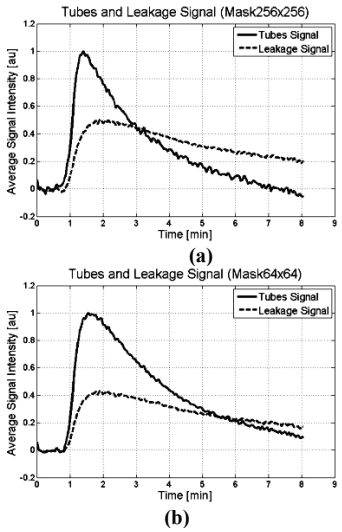

Figure 7 The intensity-time curves measured for the tubes and the leakage using the binary mask. The results for the a) high resolution and, b) low resolution datasets.

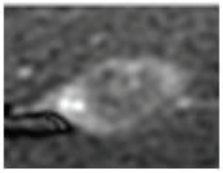

Figure 8 The region selected around the tumor for a sample frame of the in vivo DCE-MRI rabbit data

The imaging field of view was large and captured an area larger than just the tumor, thus a smaller window around the tumor (2.3x2.4cm) is selected (figure 8).

Preliminary results of applying the proposed separation method to the in vivo rabbit data is depicted in figure 9. The tumor area is segmented into two parts that correspond to the intravascular and extravascular compartments as shown in figure 9a and 9b respectively. The intensity-time curves of the two segments are shown in figure 9c.

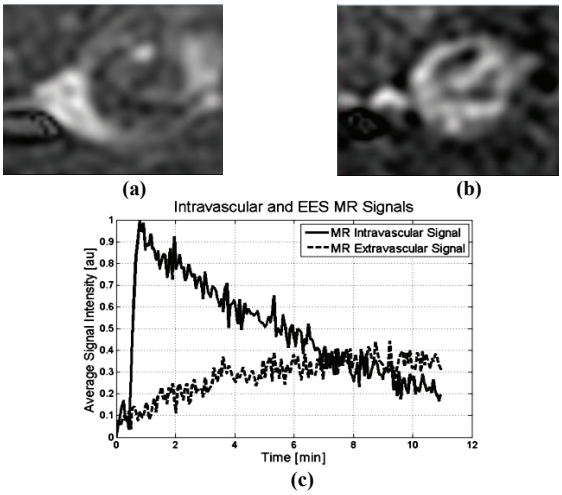

Figure 9 Results of applying ICA to the in vivo rabbit data, a) The intravascular signal (AIF), b) the extravascular signal (ES), c) the intensity-time curve corresponding to the two compartments.

4. DISCUSSION

Simulation study was performed to study the feasibility of identifying the two spaces (the tubes and the gel). Furthermore, with the simulation study we investigated the effect of resolution performance of the separation technique using the high and low resolution datasets.

As shown in Figure 5 and 6, ICA is capable of separating the two spaces in the dynamic dataset. In the low resolution case it is difficult to differentiate between the two spaces in spatial domain (Figure 3b) whereas in the temporal domain their time courses are similar to and have high correlation with those the high resolution dataset.

Figure 6 shows the actual intensity-time curves that are measured using the binary mask. As can be inferred from comparing these curves with the ones that are extracted using ICA, the curves are very similar showing that ICA curves are a very good approximation of these curves. As

reported in table 1 the ratio of the peak value of AIF to ES signal is very close in actual and ICA results. Furthermore, the FWHM, time to peak and onset time of the ICA curves are very close to those of the actual curves (table 2).

The difference between the curves as we reduce the resolution is due to the fact that in low resolution dataset the two spaces are more combined than the high resolution ones and as a result the tubes curves approach the leakage curves, which can be seen in both ICA results and the actual curves. The curves in two cases are very similar to each other and also the curves between the low and high resolution dataset are similar to each other, thus this method is capable of robustly separating the tube signal from the leakage signal.

In the in-vivo study preliminary results show that the ICA based separation technique is capable of identifying the intravascular and extravascular spaces. Comparing the AIF with the curve that was generated using Ultrasound images that used microbubbles as contrast agent (not shown), showed that the extracted intravascular curve of MR follows that of the Ultrasound data. However more data and study are necessary to evaluate the performance of the technique.

5. CONCLUSIONS

In a two compartmental PK model of a tumor, a key step is the differentiation of the signal that is produced in the feeding blood vessels (AIF) from the ES signal. We constructed an experimental phantom to mimic the behavior of real tissues which was comprised of a 10×10 grid of dialysis tubings that are surrounded by agar. The phantom was made such that contrast agent could leak from the tubes into the gel. A high resolution binary mask was constructed using a pre-contrast image of the phantom. The mask was used to separate the tubes from the gel and its results were used as the actual values for the intensity-time curves.

ICA was applied to the DCE-MRI images of the phantom to generate an automatic mask for separating the AIF and ES signals. Two different datasets were constructed with different resolutions to account for different resolution images that might be acquired in clinical trial and also to demonstrate the robustness of the method. Comparing the results of ICA with the actual curves showed that ICA was capable of separating the two spaces with high accuracy and results in intensity-time curves that were measured exactly at the tissue. Preliminary results of applying the technique to in vivo data were also promising.

6. ACKNOWLEDGEMENTS

The authors thank the Natural Sciences and Engineering Research Council of Canada (NSERC) and Ontario Institute for Cancer Research (OICR) for funding this work.

7. REFERENCES

[1] E. M. Van Cann, M. Rijpkema, A. Heerschap, A. van der Bilt, R. Koole and P. J. W. Stoelinga, "Quantitative dynamic contrast-enhanced MRI for the assessment of mandibular invasion by squamous cell carcinoma," *Oral Oncol.,* vol. 44, pp. 1147, 2008.

[2] G. V. Shah, N. J. Fischbein, D. Gandhi and S. K. Mukherji, "Dynamic contrast-enhanced MR imaging," *Topics in Magnetic Resonance Imaging,* vol. 15, pp. 71-77, 2004.

[3] Y. Yanagi, *et al.,* "Enhancement effects of test injection with a small amount of MR contrast medium in the oral and maxillofacial region," *Eur. J. Radiol.,* vol. 59, pp. 367-370, 2006.

[4] A. Shukla-Dave, N. Lee, H. Stambuk, Y. Wang, W. Huang, H. T. Thaler, S. G. Patel, J. P. Shah and J. A. Koutcher, "Average arterial input function for quantitative dynamic contrast enhanced magnetic resonance imaging of neck nodal metastases," *BMC Medical Physics,* vol. 9, 2009.

[5] P. Armitage, C. Behrenbruch, M. Brady and N. Moore, "Extracting and visualizing physiological parameters using dynamic contrast-enhanced magnetic resonance imaging of the breast," *Med. Image Anal.,* vol. 9, pp. 315-329, 2005.

[6] D. J. Collins and A. R. Padhani, "Dynamic magnetic resonance imaging of tumor perfusion," *IEEE Engineering in Medicine and Biology Magazine,* vol. 23, pp. 65-83, 2004.

[7] M. O. Leach, *et al*., "Assessment of antiangiogenic and antivascular therapeutics using MRI: Recommendations for appropriate methodology for clinical trials," *Br. J. Radiol.,* vol. 76, pp. S87-S91, 2003.

[8] J. Evelhoch, M. Garwood, D. Vigneron, M. Knopp, D. Sullivan, A. Menkens, L. Clarke and G. Liu, "Expanding the use of magnetic resonance in the assessment of tumor response to therapy: Workshop report," *Cancer Res.,* vol. 65, pp. 7041, 2005.

[9] S. C. Rankin, "MRI of the breast*," Br. J. Radiol.,* vol. 73, pp. 806-818, 2000.

[10] G. J. M. Parker, et al., "Experimentally-derived functional form for a population-averaged high-temporal-resolution arterial input function for dynamic contrast-enhanced MRI," *Magnetic Resonance in Medicine,* vol. 56, pp. 993-1000, 2006.

[11] M. A. G. Ballester, A. P. Zisserman and M. Brady, "Estimation of the partial volume effect in MRI," *Med. Image Anal.*, vol. 6, pp. 389-405, DEC, 2002.

[12] N. A. Thacker, D. C. Williamson and M. Pokric, "Voxel based analysis of tissue volume from MRI data," *Br. J. Radiol.,* vol. 77, pp. S114-S125, 2004.

[13] P. Comon, "Independent component analysis, A new concept?" *Signal Process*, vol. 36, pp. 287-314, 1994.

[14] H. Mehrabian, L. Lindvere, B. Stefanovic, and A. L. Martel, "A temporally constrained ICA (TCICA) technique for artery-vein separation of cerebral microvasculature*", Proc. SPIE,* vol. 7626, 762622, 2010.

[15] C. Chandrana, P. Bevan, J. Hudson, I. Pang, P. Burns, D. Plewes and R. Chopra, "Development of a platform for co-registered ultrasound and MR contrast imaging in vivo" *Phy. in Med. and Biol.* 56 (3) p.861-877, 2011.